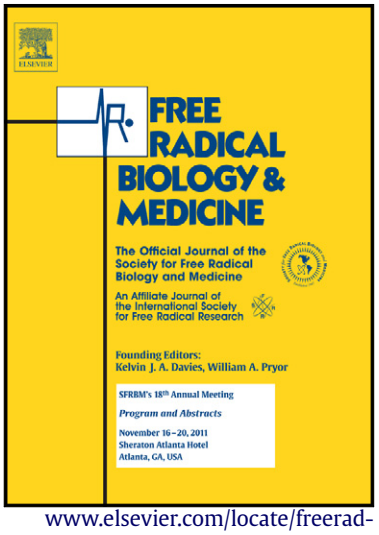

www.elsevier.com/locate/freeradbiomed

In Vivo Detection of Free Radicals using Molecular MRI and Immuno-Spin-Trapping in a Mouse Models for Amyotrophic Lateral Sclerosis (ALS)

Rheal A. Towner, Nataliya Smith, Debra Saunders, Florea Lupu, Robert Silasi-Mansat, Melinda West, Dario C. Ramirez, Sandra E. Gomez-Mejiba, Marcelo G. Bonini, Ronald P. Mason, Marilyn Ehrenshaft, Kenneth Hensley

PII: S0891-5849(13)00236-0
DOI: http://dx.doi.org/10.1016/j.freeradbiomed.2013.05.026
Reference: FRB11572

To appear in: *Free Radical Biology and Medicine*

Received date: 13 December 2012
Revised date: 13 May 2013
Accepted date: 17 May 2013

Cite this article as: Rheal A. Towner, Nataliya Smith, Debra Saunders, Florea Lupu, Robert Silasi-Mansat, Melinda West, Dario C. Ramirez, Sandra E. Gomez-Mejiba, Marcelo G. Bonini, Ronald P. Mason, Marilyn Ehrenshaft, Kenneth Hensley, *In Vivo* Detection of Free Radicals using Molecular MRI and Immuno-Spin-Trapping in a Mouse Models for Amyotrophic Lateral Sclerosis (ALS), *Free Radical Biology and Medicine,* http://dx.doi.org/10.1016/j.freeradbiomed.2013.05.026

In Vivo Detection of Free Radicals using Molecular MRI and Immuno-Spin-Trapping in a Mouse Models for Amyotrophic Lateral Sclerosis (ALS)

Running Title: *In Vivo* Radical Detection in Mouse ALS

*[1]Rheal A. Towner, [1]Nataliya Smith, [1]Debra Saunders, [2]Florea Lupu, [2]Robert Silasi-Mansat, [3]Melinda West, [4]Dario C. Ramirez, [4]Sandra E. Gomez-Mejiba, [5]Marcelo G. Bonini, [6]Ronald P. Mason, [6]Marilyn Ehrenshaft, [7]Kenneth Hensley.

[1]Advanced Magnetic Resonance Center, [2]Cardiovascular Biology, and [3]Free Radical Biology & Aging, Oklahoma Medical Research Foundation, Oklahoma City, OK 73104 U.S.A.; [4]Laboratory of Experimental Medicine & Therapeutics, Instituto Multidisciplinario de Investigaciones Biológicas-San Luis- CONICET-National University of San Luis, San Luis 5700, Argentina; [5]Departments of Medicine and Pharmacology, University of Illinois, Chicago, IL 60612 U.S.A.; [6]Laboratory of Pharmacology and Chemistry, National Institute of Environmental Health Sciences, Research Triangle Park, NC 27709 U.S.A; and [7]Department of Pathology, University of Toledo Health Sciences Campus, Toledo, OH 43614-2598 U.S.A.

*Corresponding Author:
Rheal A. Towner
Director, Advanced Magnetic Resonance Center, Oklahoma Medical Research Foundation
Oklahoma City, OK 73104 U.S.A.
Email: Rheal-Towner@omrf.org; Phone: (405) 271-7383; FAX: (405) 271-7254

Conflict of Interest:

The authors declare no competing financial interests.

Abstract:

Free radicals associated with oxidative stress play a major role in amyotrophic lateral sclerosis (ALS). By combining immuno-spin-trapping (IST) and molecular magnetic resonance imaging (mMRI), *in vivo* trapped radical adducts were detected in the spinal cords of $SOD1^{G93A}$ transgenic (Tg) mice for ALS. For this study, the nitrone spin-trap DMPO (5,5-dimethyl-1-pyrroline *N*-oxide) was administered (i.p.) over 5 days prior to administration (i.v.) of an anti-DMPO probe [anti-DMPO antibody covalently bound to an albumin (BSA)-Gd (gadolinium)-DTPA (diethylenetriamine pentaacetic acid)-biotin MRI contrast agent] to trap free radicals. MRI was used to detect the presence of the anti-DMPO radical adducts by a significant sustained increase in MR signal intensities ($p<0.05$) or anti-DMPO probe concentrations measured from T_1 relaxations ($p<0.01$). The biotin moiety of the anti-DMPO probe was targeted with fluorescent-labeled streptavidin to locate the probe in excised tissues. Negative controls included either Tg ALS mice initially administered saline rather than DMPO followed by the anti-DMPO probe, or non-Tg mice initially administered DMPO and then the anti-DMPO probe. The anti-DMPO probe was found to bind to neurons via co-localization fluorescence microscopy. DMPO adducts were also confirmed in disease/non-disease tissues from animals administered DMPO. Apparent diffusion coefficients from diffusion-weighted images of spinal cords from Tg mice were significantly elevated ($p<0.001$) compared to wild-type controls. This is the first report regarding the detection of *in vivo* trapped radical adducts in an ALS model. This novel, non-invasive, *in vivo*, diagnostic method can be applied to investigate the involvement of free radical mechanisms in ALS rodent models.

Keywords:

In vivo, Immuno-spin trapping (IST), Molecular magnetic resonance imaging (mMRI), amyotrophic lateral sclerosis (ALS), free radicals, DMPO (5,5-dimethyl-1-pyrroline-N-oxide), Gd (gadolinium)-DTPA (diethylenetriamine pentaacetic acid)-albumin-anti-DMPO-biotin probe (anti-DMPO probe)

Abbreviations:

Ab = antibody
ALS = amyotrophic lateral sclerosis
ADC = apparent diffusion coefficient
BBB = blood-brain-barrier
DWI = diffusion-weighted imaging
DMPO = 5,5-dimethyl-1-pyrroline-N-oxide
ESR = electron spin resonance
Gd-DTPA = gadolinium diethylenetriamine pentaacetic acid
IST = immuno-spin trapping
mMRI = molecular magnetic resonance imaging
RNS = reactive nitrogen species
ROS = reactive oxygen species
SOD1 = superoxide dismutase 1
T_1 = longitudinal relaxation constant
TE = echo time
TR = repetition time

Introduction:

Non-regulated overproduction of reactive oxygen and nitrogen species (ROS/RNS) plays a crucial role in many diseases, either as modulators of signal transduction or as a cause of tissue injury. Understanding the extent and timing of events triggered by free radicals *in vivo* is important since these are major determinants of disease evolution and prognosis. Monitoring *in vivo* radicals in rodent neurological disease models by combining molecular magnetic resonance imaging (mMRI) and immuno-spin trapping (IST) [1,2] technologies is possible for the first time.

Numerous studies indicate that oxidative stress, a result of an imbalance in levels of ROS and anti-oxidative defense systems, plays a crucial role in amyotrophic lateral sclerosis (ALS). Evidence exists that radicals play a major role in the pathogenesis of ALS [3]. For instance, it is known that oxidative DNA damage [8-hydroxy-2-deoxyguanosine (8-OHdG)] is elevated in the spinal cords of human-SOD1^{G93A} transgenic (Tg) mice compared to wild-type mice [4,5]. It has also been demonstrated that 4-hydroxy-2-nonenal (HNE)-modified proteins are formed in SOD1^{G93A} Tg mice [6]. It is thought that highly reactive aldehydes, including HNE, are generated from the peroxidation of cellular membrane lipids or circulating lipoproteins [6]. Protein carbonyls, which may result from reactive aldehydes, are also elevated in spinal cords of SOD1^{G93A} mice compared to controls [7]. Oxidative damage to proteins also occurs in spinal cords of ALS patients [8]. It is suggested that oxidized Cu,Zn-superoxide dismutase (SOD1) [9,10] or neurofilament light polypeptide 68 kDa [8] may be toxic to motor neurons and contribute to ALS pathogenesis. ROS/RNS may directly oxidize nucleic acids, proteins, carbohydrates and lipids, causing intracellular and intercellular perturbations in homeostasis, including DNA mutations and interference with DNA repair [11]. High concentrations of lipid-derived electrophilic products readily react with proteins, DNA and phospholipids, generating intra- and intermolecular toxic covalent adducts that lead to the propagation and amplification of oxidative stress [11].

Free radicals generated as a result of oxidative stress processes can be tagged by 5,5-dimethyl-1-pyrroline *N*-oxide (DMPO) to form DMPO-radical adducts, which can be further assessed by immuno-spin trapping (IST), a method that utilizes an antibody against DMPO [1,2,12-14]. It would be important if the formation of oxidation products could be assessed *in vivo* and cause-consequence relationships could be drawn from specific oxidative events. This would allow the correlation of the detection of real time oxidative stress markers with specific longitudinal pathological conditions associated with a particular disease.

mMRI relies on specific labelling of extracellular cell surface receptors or antigens with a targeted contrast agent. The MRI contrast agent probe is targeted to a specific receptor or antigen by an antibody (Ab). These compounds alter proton magnetization relaxation times at their sites of accumulation, making them ideal for diagnostic purposes. Paramagnetic gadolinium (Gd)-based MR

contrast agents generate a positive signal contrast (T_1 contrast) which enhances MR signal intensities of water molecules that surround these agents in T_1-weighted MR images. Gadolinium (Gd)-based probes that bind to affinity molecules have recently become popular when used with mMRI. Our laboratory has previously used mMRI methodology to provide *in vivo* evidence regarding the detection of elevated levels of various tumor markers [15-19] in glioma models. Of related importance to this study, we recently used the anti-DMPO probe to assess radical formation in a mouse diabetes model [20]. Here we have used a Gd-based, anti-DMPO probe with MRI detection to image membrane-associated radical adducts in a mouse model for ALS.

In a novel approach, we have combined the morphological image resolution of molecular MRI (mMRI) with the use of a Gd-DTPA-albumin-based contrast agent (see Fig. 1A) for signal detection with the specificity of Abs for DMPO-radicals (anti-DMPO probe) to detect *in vivo* free radicals (see Fig. 1B). The anti-DMPO probe was used to assess *in vivo* free-radical formation within spinal cords of $SOD1^{G93A}$ mice.

Methods:

Syntheses of DMPO-specific MRI contrast agents:

To recognize the DMPO-protein/lipid radicals, a mouse monoclonal anti-DMPO antibody bound to a contrast agent was used. The macromolecular contrast material, biotin-BSA-Gd-DTPA, was prepared using a modification of the method of Dafni *et al* [21]. The biotin moiety in the contrast material was added to allow histological localization. Biotin-BSA-Gd-DTPA was synthesized as described in Towner *et al*. [15]. Bovine serum albumin (BSA, Sigma) was dissolved in 0.1 M sodium bicarbonate (pH 8.5). Sulfo-NHS-Biotin (Pierce) was dissolved in double distilled water (DDW) and was added to BSA while stirring. The reaction mixture was stirred for 1 h at 4°C and an additional 2 h at room temperature. The dialyzed product in 0.1 M Hepes buffer (pH 8.8) was reacted with diethylene-triamine penta acetic-acid anhydride (DTPA, Sigma) suspended in dimethyl sulfoxide (DMSO) at room temperature. DTPA was added, and the pH was adjusted (8.5) immediately after each addition with 5 N NaOH. The mixture was stirred for 2 h at 4°C and extensively dialyzed against cold 0.1 M citrate buffer (pH 6.5). Finally, gadolinium (III) chloride ($GdCl_3$, Sigma) in 0.1 M sodium acetate buffer (pH 6.0) was added gradually, and the mixture was stirred for 24 h at 4°C. The product, biotin-BSA-Gd-DTPA, was extensively dialyzed against cold citrate buffer (0.1 M, pH 6.5) and then against DDW. A solution of biotin-BSA-GdDTPA was added directly to the solution of antibody (anti-DMPO, 200 µg/mL) for conjugation through a sulfo-NHS-EDC link between albumin and antibody according to the protocol of Hermanson [22]. Sulfo-NHS was added to the solution of biotin-BSA-Gd-DTPA and EDC. The solution

was mixed and reacted for 15 min at 25°C. This activated solution was added directly to the antibody (anti-DMPO, 20 µg/mL) for conjugation. The mixture was left to react for at least 2 h at 25°C in the dark. The product was lyophilized and subsequently stored at 4ºC and reconstituted to the desired concentration for injections in phosphate buffer saline (PBS). The final amount of the product, anti-DMPO-biotin-BSA-Gd-DTPA, that was injected into the mice is estimated to be 20 µg anti-DMPO Ab/injection and 10 mg biotin-BSA-Gd-DTPA/injection. The estimated molecular weight of the anti-DMPO-biotin-BSA-Gd-DTPA probe is estimated to be 232 kDa. As a control, normal mouse-IgG (obtained from a healthy mouse population; Alpha Diagnostic International, San Antonio, TX, USA) conjugated to biotin-BSA-Gd-DTPA (control IgG contrast agent) was synthesized by the same protocol.

In Vitro Characterization of Anti-DMPO Probe:

Vials were prepared containing either primary mouse astrocytes alone, astrocytes with hydrogen peroxide (H_2O_2) and DMPO, astrocytes with H_2O_2 + DMPO + anti-DMPO probe, or water. Cells (mouse astrocytes, CC-3187, Lonza Walkersville, Inc., Walkersville, MD, USA) were grown in flasks in complete growth medium (ABM Basal Media, Lonza Walkersville Inc.) to confluency. Two to three hours before treatment, the growth medium was replaced with serum-free medium. DMPO (40 mM) was added to appropriate vials, and after 15 min equilibrium, H_2O_2 (50 µM) was added. In the samples that contained all components, the anti-DMPO probe was added (2 µg, based on antibody calculation), and cells were incubated for 45 min. Following incubation, cells were collected, washed with PBS, centrifuged (3,000 rpm), and the pellet was resuspended in PBS for MR imaging.

Animal Experiments:

All animal experiments were conducted in accordance with the National Institutes of Health animal use and welfare guidelines and with the authorization of the institutional animal ethics committee.

As a model for ALS, a human-SOD1^{G93A} Tg mouse model (Jackson Laboratories, Bar Harbor, ME, USA; strain B6SJL-TGN-(SOD1 G93A)-1-Gur) was used which expresses human SOD1, in addition to normal murine SOD1. The SOD^{G93A} Tg mice were compared to a non-Tg control (B6SJLF2) mice which express only murine SOD1. Transgenic mice were maintained in the hemizygous state by mating SOD1^{G93A} males with B6SJL-TGN females. The G93A mutation in SOD1 is representative of a mutation found in 20-30% of familial ALS (FALS) patients [23,24]. The SOD1^{G93A} Tg mice start developing protein oxidation at ~90 days, with a substantial increase at ~115 days. Mice (n=5 SOD1^{G93A} mice) were given the anti-DMPO probe at 120 days of age. DMPO treatment commenced at 115 days to maximize the spin trapping of protein radicals prior to detection of DMPO-protein/lipid

nitrone adducts at 120 days. For controls, $SOD1^{G93A}$ mice (n=5) were administered saline instead of DMPO, while non-transgenic mice (n=5) received DMPO.

For diffusion studies, a total of 15 $SOD1^{G93A}$ mice (n=5 for each of three time-points at 85, 110 and 120 days of age) and a total of 5 non-Tg mice (120 days of age) were used.

DMPO Administration:

DMPO (1.8 mM in saline; 125 µl volume) was administered i.p. 3 x daily (every 6 hours) for 5 days. DMPO administration started at 115 days of age. No untoward effects (e.g. hypothermia, weight loss, pain at injection site, etc.) were observed following the DMPO injection period or upon necropsy.

Magnetic Resonance Techniques:

For the *in vitro* study, signal intensities were obtained using FLASH (Fast Low Angle SHot) [repetition time (TR) 125.3 ms, echo time (TE) 6.0 ms, 256 x 128 matrix, 4 steps per acquisition, 4.00 x 4.00 cm^2 field of view (FOV), 1 mm slice thickness]. T_1 maps were obtained using a RARE (Rapid Aquisition variable TR sequence (TR 200, 400, 800, 1200 and 1600 ms; TE 15 ms; 256 x 256 matrix; 2 steps per acquisition; 4.00 x 4.00 cm^2 FOV; slice thickness 1.0 mm). Pixel-by-pixel relaxation maps were reconstructed from a series of T_1-weighted images using a nonlinear two-parameter fitting procedure.

For animal studies, MR experiments were carried out under general anesthesia (1-2% Isoflurane, 0.8-1.0 L/min O_2). MR equipment included a Bruker Biospec 7.0 Tesla/30 cm horizontal-bore imaging spectrometer. Anesthetised (2% Isoflurane), restrained mice were placed in an MR-compatible cradle and inserted in a MR probe, and their spinal cords were localised by MRI. Images were obtained using a Bruker S116 gradient coil (2.0 mT/m/A) and a 72 mm quadrature multi-rung RF coil. Mice were imaged at 120 days of age.

For the mouse anti-DMPO study, multiple spinal cord ^{1}H-MR images were taken in the sagittal plane using FLASH [TR: 150.0 ms, TE: 6.0 ms, 256 x 128 matrix, 6 steps per acquisition, 5.00 x 2.56 cm^2 FOV, 1 mm slice thickness]. Mouse spinal cords were imaged at 0 (pre-contrast), 20, 40, 60, 120 and 180 min intervals post-contrast agent injection. Mice were injected intravenously with anti-DMPO or nonimmune-IgG antibodies tagged with a biotin-Gd-DTPA-albumin-based contrast agent (200 µL/kg; 1 mg antibody/kg; 0.4 mmol Gd^{+3}/kg) [15]. T_1-weighted images were obtained using a variable TR (repetition time) spin-echo sequence. Pixel-by-pixel relaxation maps were reconstructed from a series of T_1-weighted images using a nonlinear, two-parameter fitting procedure. The T_1 value of a specified region-of-interest (ROI) was computed from all the pixels in the ROI by the following equation [25] (processed by ParaVision 4.0, Bruker): $S(TR) = S_0(1 - e^{-TR/T1})$, where TR is the repetition time (ms), S_0

is the signal intensity (integer machine units) at TR>>T_1 and TE=0, and T_1 is the constant of the longitudinal relaxation time (ms). Relative probe (contrast agent) concentrations, C (M), were calculated for each of the selected ROIs using the following formula [25]: $C \propto [1/T_1(\text{after}) - 1/T_1(\text{before})]$, where $1/T_1$ (after) is the T_1 rate taken at different time points after injection of probes, and $1/T_1$ (before) is the T_1 rate taken before injection of probes.

For the diffusion-weighted study, multiple spinal cord ^{1}H-MR image slices were taken in the saggital plane using a multi-echo multi-slice, spin echo [TR 1.0 s, TE 11.61 ms (effective TE of 17.41 and 52.24 ms), 256 x 256 matrix, 4 steps per acquisition, 4.00 x 2.31 cm^2 FOV, 1 mm slice thickness]. DW images were taken using a DWI-SE pulse sequence (TR 1.0 s, TE 64.9 ms, Big delta 40.0 ms, diffusion gradient duration 2.00 ms, 184 x 96 matrix, 6 steps per acquisition, 1.0 mm slick thickness). The diffusion gradient strengths were 5.0, 20.0, 35.0 and 70.0 mT/m. The apparent diffusion coefficient (ADC) was measured by fitting the logarithm of the relative signal intensity of the lumbar region of the spinal cord tissue to the b-values, where the measured slope is the ADC.

Excised tissues:

The spinal cord was extracted as follows: mice were euthanized with CO_2, the muscles along the spine were cut, the vertebrae were cracked with rongeurs, the upper half of the vertebral column was separated from the lower half, and then the spinal cord was removed.

Immunohistochemistry:

After the spinal cords were excised, they were cut and fixed in Z-fixative (Zinc Formalin: Formaldehyde 10%, Zinc Sulfate hepatahydrate 1%) which enhances immuno-preservation. The spinal cords were then washed with PBS and incubated with 15% sucrose before embedding in Optimal Cutting Temperature (O.C.T.) compound and frozen in liquid nitrogen. Immunohistochemical staining of DMPO-protein/lipid nitrone adducts was done by incubating tissue sections with anti-DMPO antibodies conjugated to fluorescein isothiocyanate (FICT) in phosphate-buffered saline containing 0.1% v/v saponin. To target the Gd-based anti-DMPO probe in fixed tissues, which were previously studied *in vivo* for molecular MRI studies, cryosections were stained with Cy3-labelled streptavidin (016-160-085, Jackson ImmunoResearch Laboratories, Inc., West Grove, PA, USA), which binds to the biotin moiety of the albumin-Gd-DTPA-biotin contrast agent within the target tissue. For fluorescence staining of the endothelial marker, CD31, a rat anti-mouse monoclonal antibody (PECAM-1, 550274, BD Biosciences, San Jose, CA, USA) was used, along with a donkey anti-rat FITC secondary antibody (712-095-153, Jackson ImmunoResearch Laboratories). For fluorescence staining of the neuronal marker, NrCAM, a rabbit polyclonal antibody (anti-NRCAM, ab24344, Abcam, Cambridge, MA, USA) that reacts against

mouse, rat and human was used, along with a donkey anti-rabbit FITC (711-095-152, Jackson ImmunoResearch Laboratories). Stained tissue slices were examined with a Nikon C1 confocal laser scanning microscope (Nikon Instruments, USA).

Statistical Analyses:

Statistical differences between the probe-administered and control groups were analyzed with a one-way ANOVA and a post-hoc Tukey's multiple comparisons test using commercially available software (InStat; GraphPad Software, San Diego, CA). A *p* value of < 0.05 was considered to indicate a statistically significant difference.

Results:

In vitro T_1 relaxation values for oxidative-stress-exposed mouse astrocytes in the presence of the anti-DMPO probe are shown in Figure 2. T_1 relaxation was found to significantly decrease in vials containing mouse astrocytes exposed to hydrogen peroxide to form radicals that were trapped with DMPO and then tagged with the anti-DMPO probe compared to primary astrocytes alone ($p<0.01$), astrocytes with hydrogen peroxide and DMPO ($p<0.01$), or water alone ($p<0.0001$), indicating the specific detection of cells with membrane-associated radicals; in effect low molecular weight radicals trapped with DMPO, were washed away prior to MR imaging.

When mMRI and a Gd-based, anti-DMPO molecular-targeting probe were used in a mouse model for ALS, the MR signal intensities increased in the lumbar region of the spinal cords obtained from T_1-weighted MR images (see Fig. 3) compared to controls consisting of ALS mice administered saline instead of DMPO and wild-type mice administered DMPO and the anti-DMPO probe. The difference images between pre- and 120 min post-administration of the anti-DMPO probe depict hypointense regions in the ALS mouse spinal cords (see Fig. 3Aiv). Figure 3 (Aiii, Aiv, Bi, and Bii) depicts the specific uptake of the anti-DMPO probe in the spinal cord regions of a transgenic mouse model for ALS, as illustrated by an increase in signal intensity in the lumbar region (red oval) shown in the difference image [120 min post- minus pre-administration of the anti-DMPO probe) (Fig. 3Aiv or Bii)]. Quantification of SI differences are shown in Fig. 3D, indicating significantly higher MRI signals in the ALS mice administered the anti-DMPO probe compared to the ALS mice administered saline instead of DMPO (**$p<0.01$) or the non-ALS wild-type mice with the anti-DMPO probe (*$p<0.05$). Figure 3E shows the estimated anti-DMPO probe concentrations in ALS mice initially administered DMPO followed by the anti-DMPO probe in the lumbar regions of mouse spinal cords as calculated from T_1 relaxation differences between post- and pre- probe administration. Estimated anti-DMPO probe

concentrations were found to be $10.3 \pm 1.4 \times 10^{-5}$ M in ALS mice, which were significantly increased ($p<0.0001$) compared to controls (ALS mice given saline instead of DMPO and the anti-DMPO probe (ALS-C): $3.8 \pm 0.5 \times 10^{-5}$ M; or wild-type mice given both DMPO and the anti-DMPO probe (non-ALS-D): $4.1 \pm 0.6 \times 10^{-5}$ M).

Fluorescence detection of the anti-DMPO probe is shown in Fig. 4 (B). The fluorescent areas observed are due to the presence of the anti-DMPO probe, which is detected in the spinal cords (lumbar region; rectangular ROI) of only the ALS mice and not the non-Tg mice (Fig. 4A). Co-localization images of the anti-DMPO probe with the endothelial marker, CD31, or a neuronal marker, NrCAM, are shown in Figs. C and D, respectively. The anti-DMPO probe (red fluorescence) seems to be not co-localized with CD31 (green fluorescence) (Figs. Ci and ii), however there is co-localization (due to presence of yellow from combined red (anti-DMPO probe) and green (neuronal marker)) with the neuronal marker, NrCAM (Figs. Di and ii).

IHC detection of DMPO-nitrone adducts in spinal cords of non-ALS and ALS mice are shown in Fig. 5. A comparison of DMPO-adduct fluorescence images in a saline-treated (no DMPO) ALS mouse (Figs. 5Ai and ii) versus a ALS mouse spinal cord (Figs. 5Bi and ii) indicates that only the ALS mouse treated with DMPO had increased levels of DMPO-adducts.

Figure 6 depicts morphological T_2-weighted images and diffusion-weighted images of non-Tg controls and ALS mice (Fig. 5A-C) as well as calculated apparent diffusion coefficients (ADC) for controls compared to ALS mice at 85, 105 and 120 days of age during disease progression. Both the T_2-weighted MR images and the DW images indicate increased signal intensities in the lumbar region of the spinal cord. ADC values (Fig. 5E) become elevated as the disease progresses, with a significant increase in ADC at 120 days of age for ALS mice compared to controls ($p<0.001$) as well as a significant increase at 120 days for ALS mice compared to earlier stages of the disease at 85 days ($p<0.01$).

Discussion:

Once formed, macromolecular radicals react with nitrone spin traps producing nitroxide radicals via a process called spin trapping. It is anticipated that only radical adducts that are membrane-associated (e.g. protein and/or lipid radical adducts) will be targeted by the Gd-based, anti-DMPO probe and detected by MRI, as any soluble DMPO-adducts will be metabolized and excreted, and the probe construct was designed primarily for detecting primarily receptors or targets on a cell membrane. Also in order to more widely distribute the probe through blood vessels following intravenous injection albumin was added to the probe construct. The biotin moiety adds another option for conducting *ex vivo*

florescence imaging for the same probe used in the mMRI evaluations. Although *in vivo* free radical concentrations can not be determined absolutely from this study, estimated anti-DMPO probe concentrations, which are proportional to levels of free radicals that react with DMPO, were found to be significantly increased ($p<0.0001$), ~2-fold in ALS mice compared to controls [ALS mice given saline instead of DMPO and the anti-DMPO probe or non-Tg mice given both DMPO and the anti-DMPO probe) (Fig. 3)].

Since it is thought that the anti-DMPO probe mainly targets the cell surface, we speculate that cell membrane-associated protein or lipid radicals that are trapped by DMPO could form protein- or lipid-radical-DMPO adducts that can be detected by the anti-DMPO probe. However, it is possible that the anti-DMPO probe could reach beyond the cell surface. For instance, we have previously published results using a similar probe construct for assessing *in vivo* levels of inducible nitric oxide synthase (iNOS), where in that study, transmission electron microscopy (TEM) of gold-labeled anti-iNOS antibody was found to be located in the plasma membrane of rat C6 glioma cells taken from an intracellular tumor [16]. As we detected *in vivo* levels of iNOS in C6 rat gliomas with mMRI, we can surmise that some of the anti-iNOS probe that was detected was located in the plasma membrane, and therefore possibly some of the anti-iNOS probe was taken up by the cell. In this study, co-localization fluorescence imaging data of the anti-DMPO probe and markers for endothelial cells or neurons indicates that the DMPO-trapped radicals are associated with neurons and possibly other brain tissue related cells, but not endothelial cells (Fig. 4). These images also indicate the possibility that the anti-DMPO probe is not only on the cell surface, but may also be internalized (Figs. 4Cii and Dii). Further studies to verify whether intracellular free radicals are trapped *in vivo* when the anti-DMPO probe is administered will need to be further conducted.

Previous studies have used IST to predominantly detect protein radicals *in vitro* and *ex vivo* (but not *in vivo*) using an antibody against the DMPO-nitrone adduct and microscopic fluorescence imaging. For instance, *in vitro* studies by Ramirez *et al.* utilized IST to detect protein radicals produced by the H_2O_2-induced SOD1-system in the presence of (bi)carbonate [2,12]. This system produced a diffusible carbonate radical anion that is thought to be mostly responsible for oxidizing crtitical residues, such as tryptophan, resulting in SOD1 inactivity [2,12]. In another study where oxyhemoglobin was treated with peroxynitrite or myoglobin was exposed to hydrogen peroxide, both in the presence of low DMPO concentrations, predominantly cysteine residues were detected with IST and mass spectrometry, however with high concentrations of DMPO, more tyrosyl radicals were found [26]. It is conceivable that protein and lipid radicals in cell membranes produced by reaction with initiating radicals (e.g. $^{\bullet}OH$ (hydroxyl) radicals, $^{\bullet}NO_2$ (nitrogen dioxide) or $CO_3^{\bullet-}$ (carbonate) radicals [2,27,28]) can be trapped by DMPO to form DMPO-radical adducts that could be detected by the anti-DMPO probe. It is known that

DMPO has previously been used to trap lipid radicals [29-31] and therefore IST could possibly be used to detect DMPO-lipid radical adducts.

There have been studies by Mason's group to establish if artifact formation could contribute to DMPO-radical adduct formation, and it was determined that spin trapping with DMPO provided authentic free radical signals with most substrates, and that DMPO was not very susceptible to artifacts arising from non-radical chemistry (nucleophilic addition) [32,33]. It was pointed out that only in the presence of cyanide, horseradish peroxidase and high concentrations of DMPO (100 mM), that cyanide oxidation via the Forrester-Hepburn reaction (hydroxylamine formation and subsequent oxidation) could occur *in vitro* [32,33], implying that non-radical chemistry is possible but may play a minimal role. If some non-radical oxidation did occur in biological systems, the results obtained would not affect the quantitative analysis of the data or any conclusions about the biochemical origin of the DMPO-radical adducts [32,33]. In general, as disease progresses, there should be increased binding of DMPO-radical adducts, whether obtained from radical or non-radical events, which can be detected *in vivo* by the anti-DMPO probe.

Both severe protein and lipid oxidation have been previously demonstrated in $SOD1^{G93A}$ mice [34]. It has been shown that there are elevated 3-nitrotyrosine levels in mitochondrial proteins from $SOD1^{G93A}$ astrocytes [35], spinal cords of $SOD1^{G37R}$ mice [36], as well as ALS patients [37]. It is also known that 4-hydroxy-2-nonenal (HNE)-modified proteins are elevated in the spinal cord motor neurons of $SOD1^{G93A}$ mice [6]. HNE is also elevated in the spinal cords of ALS patients [38]. Malondialdehyde (MDA), a marker of lipid peroxidation, was also found to increase in spinal cords of $SOD1^{G93A}$ mice [39]. It has also been reported that there is increased nitration and oxidation of proteins in $SOD1^{G93A}$ mouse spinal cords [40,41] and brains [42]. These findings strongly support the notion that both protein and lipid radicals may possibly react with DMPO and the resulting DMPO protein/lipid radical adducts can be recognized by the anti-DMPO probe.

Uptake of the anti-DMPO probe into spinal cord tissue is thought to be due to a disrupted blood-spinal cord barrier and blood-brain barrier (BBB). Evidence indicates that both blood spinal cord barrier and BBB are disrupted in spinal cords and brains, respectively, in $SOD1^{G93A}$ mice [43] and rats [44]. Disruption of the blood spinal cord barrier could allow the anti-DMPO probe to reach spinal cord tissue, as is supported by detection of bound anti-DMPO probe by both *in vivo* mMRI and *ex vivo* fluorescence imaging results. Previously, we used molecular MRI probes of a similar construct (Gd-DTPA-albumin-antibody-biotin) that were able to enter the leaky blood-tumor-barrier in rodent gliomas [15-17].

ALS (also known as Lou Gehrig's disease) is a fatal motor neuron disease affecting the motor cortex, brainstem and spinal cord. Familial ALS (FALS) is exhibited in 10-15% of all ALS patients, which affects some 60,000-100,000 people worldwide, with only a 1-5-year survival rate following

disease onset [23,24]. A common SOD1 mutation that is associated with FALS is G93A, where an alanine is substituted for glycine at residue 93, which is represented in 20-30% of FALS cases [24,45,46]. Human-SOD1^{G93A} mice have this mutation, and they develop severe motor neuron loss and motor weakness starting at 100 days of age until ~130 days, when extreme paralysis and death occurs. The pathogenesis of mutant SOD1 is thought to occur via the formation of carbonate radical anions, altered folding and/or malfunctioning of the protein [47,48]. There is evidence that a complex interaction between genetic and molecular factors result in damage to critical target proteins and organelles within ALS motor neurons [49]. It is also known that protein oxidative damage is strongly associated with ALS-specific changes in n-3 fatty acid concentrations, as well as mitochondrial dysfunction leading to increased free radical production [50].

In SOD^{G93A} mice, neurotoxic signaling from motor neurons is thought to promote microglial overproduction of ROS, which may then lead to motor neuron death [10]. It has been shown that astrocytes from SOD1^{G93A} mice are hypersensitive to neuroinflammatory cytokines and produce increased protein oxidation in culture compared to non-Tg or wild-type SOD1-expressing glia [51]. It has been shown that motor neurons are capable of generating peroxynitrite in ALS [52]. Mitochondrial dysfunction has been found to be a key early element in the pathogenesis of motor neuron degeneration in human-SOD1^{G93A} mice [53], rats [33,54] and humans [55]. In an *ex vivo* study by Cassina *et al*., immuno-staining for DMPO-adducts was done in the spinal cords of SOD^{G93A} rats [35]. In our study, *in vivo* membrane-bound radicals were found to be elevated primarily in the lumbar region of transgenic mice with ALS symptoms. DW imaging data also indicated increased ADC values due to tissue injury in the lumbar region of SOD1^{G93A} mice. Extensive future studies will need to be done to establish the nature of the trapped DMPO adducts, possibly by detecting and identifying specific oxidized proteins and/or lipids.

There are other imaging methods that have been used to detect radicals, including ESR, fluorescence imaging, or Overhauser-enhanced MRI (OMRI). OMRI potentially offers a method of detecting low concentrations of free radicals generated by specific biological processes; however, spatial resolution and general radical detection is limited [56]. ESR imaging is sensitive but limited to the detection of an injected paramagnetic probe at the injection site and not the general detection of a broad range of radicals. Fluorescence imaging is restricted to excised tissues or isolated cells.

Here we combined mMRI and IST to show, for the first time, noninvasive, *in vivo* detection of spin-trapped radicals in a mouse model for ALS. Using both mMRI and IST provides the advantage of *in vivo* image resolution and spatial differentiation of regional events in heterogeneous tissues or organs, and the regional targeting of free radical-mediated oxidation in a disease process. This method can be applied to any radical-associated neuro-pathological condition for the *in vivo* diagnosis of

macromolecular protein and/or lipid radical levels, particularly if there is increased BBB or blood spinal cord barrier permeability.

Acknowledgements:

Funding was obtained by the Oklahoma Medical Research Foundation (RAT), the National Institute of Environmental Health Sciences (NIEHS) (RPM), the Muscular Dystrophy Association (KH), and the Judith and Jean Pape Adams Charitable Foundation (KH). We would like to thank Dr. Yasvir Tesiram (currently at the Univ. of Queensland, Brisbane, Qld., Australia) for assistance in optimization of the DWI pulse sequence, and Mr. Haitham Abd El-Moaty (currently at Texas Southern Univ.) for assisting in data acquisition for the DWI study.

References:

[1] Mason, R.P. Using anti-5,5-dimethyl-1-pyrroline N-oxide (anti-DMPO) to detect protein radicals in time and space with immune-spin trapping. Free Radic. Biol. Med. 36: 1214-23; 2004.

[2] Ramirez, D.C.; Gomez-Mejiba, S.E.; Corbett, J.T.; Deterding, L.J.; Tomer, K.B.; Mason, R.P. Cu, Zn-superoxide dismutase-driven free radical modifications: copper- and carbonate radical anion-initiated protein radical chemistry. Biochem. J. 417:341-53; 2009.

[3] Garbuzova-Davis, S.; Saporta, S.; Haller, E.; Kolomey, I.; Bennett, S.P.; Potter, H.; Sanberg, P.R. Evidence of compromised blood-spinal cord barrier in early and late symptomatic SOD1 mice modeling ALS. PLoS One 2: e1205; 2007.

[4] Warita, H.; Hayashi, T.; Murakami, T.; Manabe, Y.; Abe, K. Oxidative damage to mitochondrial DNA in spinal motoneurons of transgenic ALS mice. Brain Res. Mol. Brain Res. 89: 147-52; 2011.

[5] Aguirre, N.; Beal, M.F.; Matson, W.R.; Bogdanov, M.B. Increased oxidative damage to DNA in an animal model of amyotrophic lateral sclerosis. Free Radic. Res. 39: 383-8; 2005.

[6] Perluigi, M.; Fai Poon, H.; Hensley, K.; Pierce, W.M.; Klein, J.B.; Calabrese, V.; De Marco, C.; Butterfield, D.A. Proteomic analysis of 4-hydroxy-2-nonenal-modified proteins in G93A-SOD1 transgenic mice: a model of familial amyotrophic lateral sclerosis. Free Radic. Biol. Med. 38: 960-8; 2005.

[7] Hensley, K.; Floyd, R.A.; Gordon, B.; Mou, S.; Pye, Q.N.; Stewart, C.; West, M.; Williamson, K. Temporal patterns of cytokine and apoptosis-related gene expression in spinal cords of the G93A-SOD1 mouse model of amyotrophic lateral sclerosis. J. Neurochem. 82: 365-74; 2002.

[8] Niebroj-Dobosz, I.; Dziewulska, D.; Kwiecinski, H. Oxidative damage to proteins in the spinal cord in amyotrophic lateral sclerosis (ALS). Folia Neuropatholol. 42: 151-6; 2004.

[9] Kabashi, E.; Valdmanis, P.N.; Dion, P.; Rouleau, G.A. Oxidized/misfolded superoxide dismutase-1: the cause of all amyotrophic lateral sclerosis? Ann. Neurol. 62: 553-9; 2007.

[10] Appel, S.H.; Zhao, W.; Beers, D.R.; Henkel, J.S. The microglial-motoneuron dialogue in ALS. Acta. Myol. 30: 4-8; 2011.

[11] Federico, A.; Morgillo, F.; Tuccillo, C.; Ciardiello, F.; Loguercio, C. Chronic inflammation and oxidative stress in human carcinogenesis. Int. J. Cancer 121: 2381-6; 2007.

[12] Ramirez, D.C.; Gomez Mejiba, S.E.; Mason, R.P. Mechanism of hydrogen peroxide-induced Cu, Zn-superoxide dismutase-centered radical formation as explored by immune-spin trapping: the role of copper- and carbonate radical anion-mediated oxidations. Free Radic. Biol. Med. 38: 201-14; 2005.

[13] Detweiler, C.D.; Deterding, L.J.; Tomer, K.B.; Chignell, C.F.; Germolec, D.; Mason, R.P. Immunological identification of the heart myoglobin radical formed by hydrogen peroxide. Free Radic. Biol. Med. 33: 364-9; 2002.

[14] Gomez-Mejiba, S.E.; Zhai, Z.; Akram, H.; Deterding, L.J.; Hensley, K.; Smith, N.; Towner, R.A.; Tomer, K.B.; Mason, R.P.; Ramirez, D.C. Immuno-spin trapping of protein and DNA radicals: “tagging” free radicals to locate and understand the redox process. Free Radic. Biol. Med. 46: 853-65; 2009.

[15] Towner, R.A.; Smith, N.; Tesiram, Y.; Garteiser, P.; Saunders, D.; Cranford, R.; Silasi-Mansat, R.; Herlea, O.; Ivanciu, L.; Wu, D.; Lupu, F. *In vivo* detection of c-Met expression in a rat C6 glioma model. J. Cellular Molecular Med. 12:174-186; 2008.

[16] Towner, R.A.; Smith, N.; Doblas, S.; Garteiser, P.; Watanabe, Y.; He, T.; Saunders, S.; Herlea, O.; Silasi-Mansat, R.; Lupu, F. *In vivo* detection of inducible nitric oxide synthase (iNOS) in rodent gliomas. Free Radic. Biol. Med. 48: 691-703; 2010.

[17] He, T.; Smith, N.; Saunders, D.; Doblas, S.; Hoyle, J.; Silasi-Mansat, R.; Lupu, F.; Lerner, M.; Brackett, D.J.; Towner, R.A. Molecular MRI assessment of vascular endothelial growth factor receptor-2 in a rat C6 glioma model. J. Cell. Molec. Med. 15: 837-849; 2011.

[18] Towner, R.A.; Smith. N.; Asano, Y.; Doblas, S.; Saunders, D. Molecular MRI approaches used to aid in the understanding of the tissue regeneration marker Met *in vivo*: implications for tissue engineering. Tissue Eng. Part A 16: 365-371; 2010.

[19] Towner, R.; Smith, N.; Asano, Y.; He, T.; Doblas, S.; Saunders, D.; Silasi-Mansat, R.; Lupu, F.; Seeney, C.E. Molecular MRI approaches used to aid in the understanding of angiogenesis *in vivo*: implications for tissue engineering. Tissue Eng. Part A 16: 357-364; 2010.

[20] Towner, R.A.; Smith, N.; Saunders, D.; Henderson, M.; Downum, K.; Lupu, F.; Silasi-Mansat, R.; Ramirez, D.C.; Gomez-Mejiba, S.E.; Bonini, M.G.; Ehrenshaft, M.; Mason, R.P. *In vivo* imaging of immunospin-trapped radicals with molecular magnetic resonance imaging in a mouse diabetes model. Diabetes 61: 2405-13; 2012.

[21] Dafni, H.; Landsman, L.; Schechter, B.; Kohen, F.; Neeman, M. MRI and fluorescence microscopy of the acute vascular response to VEGF165: vasodilation, hyper-permeability and lymphatic uptake, followed by rapid inactivation of the growth factor. NMR in Biomedicine, 15: 120-131; 2002.

[22] Hermanson, G. Bioconjugate Techniques. Academic Press, New York, pp. 456-493, 494-527; 1996.

[23] Cudkowicz, M.E.; McKena-Yaske, R.N.; Sapp, P.E.; Chin, W.; Geller, B.S.; Hayden, D.L.; Schoenfeld, D.A.; Hosler, B.A.; Horvitz, H.R.; Brown, R.H. Epidemiology of mutations in superoxide dismutase in amyotrophic lateral sclerosis. Ann. Neurol. 41: 210-21; 1997.

[24] Orrel, R.W. Amyotrophic lateral sclerosis: copper/Zinc superoxide dismutase (SOD1) gene mutations. Neuromus. Disord. 10: 63-8; 2000.

[25] Haacke, E.M.; Brown, R.W.; Thompson, M.R.; Venkatesan, R. Magnetic resonance imaging: physical principles and sequence design. Wiley-Liss; 1999.

[26] Bhattacharajee, S.; Deterding, L.J.; Jiang, J.; Bonini, M.G.; Tomer, K.B.; Ramirez, D.C.; Mason, R.P. Electron transfer between a tyrosyl radical and a cysteine residue in hemoproteins: spin trapping analysis. J. Am. Chem. Soc. 129: 13493-501; 2007.

[27] Bonini, M.G.; Gabel, S.A.; Ranguelova, K.; Stadler, K.; Derose, E.F.; London, R.E.; Mason, R.P. Direct magnetic resonance evidence for peroxymonocarbonate involvement in the Cu,Zn-superoxide dismutase peroxidase catalytic cycle. J. Biol. Chem. 284: 14618-27; 2009.

[28] Medinas, D.B.; Augusto, O. Mechanism of the peroxidase activity of superoxide dismutase 1. Free Radic. Biol. Med. 49: 682; 2010.

[29] Chamulitrat, W.; Jordan, S.J.; Mason, R.P. Fatty acid radical formation in rats administered oxidized fatty acids: *in vivo* spin trapping investigation. Arch. Biochem. Biophys. 299: 361-367; 1992.

[30] Dikalov, S.I.; Mason, R.P. Spin trapping of polyunsaturated fatty acid-derived peroxyl radicals: reassignment to alkoxyl radical adducts. Free Radic. Biol. Med. 30: 187-197; 2001.

[31] Reis, A.; Domingues, P.; Ferrer-Correla, A.J.; Domingues, M.R. Identification of free radicals of glycerophosphatidylcholines containing omega-6 fatty acids using spin trapping coupled with tandem mass spectrometry. Free Radic. Res. 41: 432-443; 2007.

[32] Leinisch, F.; Ranguelova, K.; DeRose, E.F.; Jiang, J.J.; Mason, R.P. Evaluation of the Forrester-Hepburn mechanism as an artefact source in ESR spin trapping. Chem. Res. Toxicol. 24: 2217-2226; 2011.

[33] Ranguelova, K.; Mason, R.P. The fidelity of spin trapping with DMPO in biological systems. Magn. Reson. Chem. 49: 152-158; 2011.

[34] Hensley, K.; Mhatre, M.; Mou, S.; Pye, Q.N.; Stewart, C.; West, M.; Williamson, K.S. On the relation of oxidative stress to neuroinflammation: lessons learned from the G93A-SOD1 mouse model of amyotrophic lateral sclerosis. Antioxidants Redox Signaling 8: 2075-87; 2006.

[35] Cassina, P.; Cassina, A.; Pehar, M.; Castellanos, R.; Gandelman, M.; de León, A.; Robinson, K.M.; Mason, R.P.; Beckman, J.S.; Barbeito, L.; Radi, R. Mitochondrial dysfunction in $SOD1^{G93A}$-bearing astrocytes promotes motor neuron degeneration: prevention by mitochondrial-targeted antioxidants. J. Neurosci. 28: 4115-22; 2008.

[36] Bruijn, L.I.; Beal, M.F.; Becher, M.W.; Schulz, J.B.; Wong, P.C.; Price, D.L.; Cleveland, D.W. Elevated free nitrotyrosine levels, but not protein-bound nitrotyrosine or hydroxyl radicals, throughout amyotrophic lateral sclerosis (ALS)-like disease implicate tyrosine nitration as an aberrant in vivo property of one familial ALS-linked superoxide dismutase 1 mutant. Proc. Natl. Acad. Sci. U.S.A. 94: 7606-11; 1997.

[37] Beal, M.F.; Ferrante, R.J.; Browne, S.E.; Matthews, R.T.; Kowall, N.W.; Brown, R.H. Jr. Increased 3-nitrotyrosine in both sporadic and familial amyotrophic lateral sclerosis. Ann. Neurol. 42: 644-54; 1997.

[38] Zarkovic, K. 4-hydroxynonenal and neurodegenerative diseases. Mol. Aspects Med. 24: 293-303; 2003.

[39] Fang, L.; Teuchert, M.; Huber-Abel, F.; Schattauer, D.; Hendrich, C.; Dorst, J.; Zettlmeissel, H.; Wlaschek, M.; Scharffetter-Kochanek, K.; Kapfer, T.; Tumani, H.; Ludolph, A.C.; Brettschneider, J. MMP-2 and MMP-9 are elevated in spinal cord and skin in a mouse model of ALS. J. Neurological Sci. 294: 51-56; 2010.

[40] Casoni, F.; Basso, M.; Massignan, T.; Gianazza, E.; Cheroni, C.; Salmonia, M.; Bonetto, V. Protein nitration in a mouse model of familial amyotrophic lateral sclerosis: possible multifunctional role in the pathogenesis. J Biol Chem 280: 16295–16304; 2005.

[41] Basso, M.; Samengo, G.; Nardo, G.; Massignan, T.; D'Alessandro, G.; Tartari, S.; Cantoni, L.; Marino, M.; Cheroni, C.; De Biasi, S.; Giordana, M.T.; Strong, M.J.; Estevez, A.G.; Salmona, M.; Bendotti, C.; Bonetto, V. Characterization of detergent-insoluble proteins in ALS indicates a causal link between nitrative stress and aggregation in pathogenesis. PLoS One. 4:e8130; 2009.

[42] Liu D, Bao F, Wen J, Liu J. Mutation of superoxide dismutase elevates reactive species: comparison of nitration and oxidation of proteins in different brain regions of transgenic mice with amyotrophic lateral sclerosis. Neuroscience. 146:255-64; 2007.

[43] Garbuzova-Davis, S.; Rodrigues, M.C.; Hermandez-Ontiveros, D.G.; Louis, M.K.; Willing, A.E.; Borlongan, C.V.; Sanberg, P.R. Amyotrophic lateral sclerosis: a neurovascular disease. Brain Res. 1398: 113-25; 2011.

[44] Nicaise, C.; Mitrecic, D.; Demetter, P.; De Decker, R.; Authelet, M.; Boom, A.; Pochet, R. Impaired blood-brain and blood-spinal cord barriers in mutant SOD1-linked ALS rat. Brain Res. 1301: 152-62; 2009.

[45] Rosen, D.R. Mutations in Cu/Zn superoxide dismutase gene are associated with familial amyotrophic lateral sclerosis. Nature 364: 362; 1993.

[46] Hayward, C.; Brock, D.J.; Minns, R.A.; Swingler, R.J. Homozygosity for Asn86Ser mutation in the CuZn-superoxide dismutase gene produces a severe clinical phenotype in a juvenile onset case of familial amyotrophic lateral sclerosis. J. Med. Genet. 35: 174; 1998.

[47] Chou, C.M.; Huang, C.J.; Shih, C.M.; Chen, Y.P.; Liu, T.P.; Chen, C.T. Identification of three mutations in the Cu, Zn-superoxide dismutase (Cu, Zn-SOD) gene with familial amyotrophic lateral sclerosis: transduction of human Cu, Zn-SOD into PC12 cells by HIV-1 TAT protein basic domain. Ann. N.Y. Acad. Sci. 1042: 303-13; 2005.

[48] Valentine, J.S. Do oxidatively modified proteins cause ALS? Free Radic. Biol. Med. 33: 1314-20; 2002.

[49] Vucic, S.; Kiernan, M.C. Pathophysiology of neurodegeneration in familial amyotrophic lateral sclerosis. Curr. Mol. Med. 9: 255-72; 2009.

[50] Ilieva, E.V.; Ayala, V.; Jové, M.; Dalfó, E.; Cacabelos, D.; Povedano, M.; Bellmunt, M.J.; Ferrer, I.; Pamplona, R.; Portero-Otín, M. Oxidative and endoplasmic reticulum stress interplay in sporadic amyotrophic lateral sclerosis. Brain 130: 3111-23; 2007.

[51] Hensley, K.; Abdel-Moaty, H.; Hunter, J.; Mhatre, M.; Mou, S.; Nguyen, K.; Potapova, T.; Pye, Q.N.; Qi, M.; Rice, H.; Stewart, C.; Stroukoff, K.; West, M. Primary glia expressing the G93A-SOD1 mutation present a neuroinflammatory phenotype and provide a cellular system for studies of glial inflammation. J. Neuroinflam. 3:2; 2006.

[52] Sahawneh, M.A.; Ricart, K.C.; Roberts, B.R.; Bomben, V.C.; Basso, M.; Ye, Y.; Sahawneh, J.; Franco, M.C.; Beckman, J.S.; Estévez, A.G. Cu,Zn-superoxide dismutase increases toxicity of mutant and zinc-deficient superoxide dismutase by enhancing protein stability. J. Biol. Chem. 285: 33885-97; 2010.

[53] Panov, A.; Kubalik, N.; Zinchenko, N.; Hemendinger, R.; Dikalov, S.; Bonokovsky, H.L. Respiration and ROS production in brain and spinal cord mitochondria of transgenic rats with mutant G93a Cu/Zn-superoxide dismutase gene. Neurobiol. Dis. 44: 53-62; 2011.

[54] Miquel, E.; Cassina, A.; Martinez-Palma, L.; Bolatto, C.; Trías, E.; Gandelman, M.; Radi, R.; Barbeito, L.; Cassina, P. Modulation of astrocytic mitochondrial function by dichloroacetate improves survival and motor performance in inherited amyotrophic lateral sclerosis. PLoS One 7: e34776; 2012.

[55] Duffy, L.M.; Chapman, A.L.; Shaw, P.J.; Grierson, A.J. Review: the role of mitochondria in the pathogenesis of amyotrophic lateral sclerosis. Neuropathol. Appl. Neurobiol. 37: 336-52; 2011.

[56] Massot, P.; Parzy, E.; Pourtau, L.; Mellet, P.; Madelin, G.; Marque, S.; Franconi, J.M.; Thiaudiere, E. *In vivo* high-resolution 3D overhauser-enhanced MRI in mice at 0.2 T. Contrast Media Mol. Imaging 7: 45-50; 2012.

Figure Captions:

Figure 1: Approach for combined *in vivo* mMRI and IST. (A) Anti-DMPO-albumin-Gd-DTPA-biotin mMRI probe. (B) Immuno-spin trapping of protein radicals (•P) with anti-DMPO mMRI probe. DMPO is injected i.p. to trap protein/lipid radicals and generate Nitrone-Protein/Lipid adducts. Anti-DMPO is injected i.v. to target Nitrone-Protein/Lipid adducts, which can be visualized by mMRI.

Figure 2: *In vitro* assessment of the anti-DMPO probe in mouse astrocytes. (A) MRI signal intensities (SI) (T_1-weighted) and T_1 maps (T1) of vials containing either (1) astrocytes alone, (2) astrocytes + hydrogen peroxide (H_2O_2) + DMPO (A+HP+DMPO), (3) astrocytes + H_2O_2 + DMPO + anti-DMPO probe (A+HP+D+P) or (4) water. (B) T_1 relaxation values (ms) of vials containing samples 1-4 described above. Values are represented as mean ± S.D.. There was a significant decrease in T_1 relaxation for samples containing astrocytes + H_2O_2 + DMPO + anti-DMPO probe compared to astrocytes alone ($p<0.01$), astrocytes with H_2O_2 and DMPO ($p<0.01$) or water ($p<0.0001$). n=5 for all groups.

Figure 3: Molecular MRI (mMRI) detection of DMPO-trapped radical adducts (as detected by the anti-DMPO probe) in an ALS Tg mouse model. Representative T_1-weighted MR images of an ALS transgenic mouse spinal cord at pre- (Ai), 25 (Aii) and 120 min (Aiii) *in vivo* post-administration of the anti-DMPO probe. The post-contrast image obtained 120 min post-administration of the anti-DMPO probe (Aiii) and the difference image [Aiii (image at 120 min post-administration of anti-DMPO probe) minus Ai (pre-administration image)] (iv) show an enhanced region (dark gray areas) in the lumbar region of the spinal cord (red oval region). (B) Difference images obtained from images at 120 min post-administration of the anti-DMPO probe minus the pre-administration image [raw MR image (i), and thresholded image (ii)] of an ALS mouse (ALS-D) administered the anti-DMPO probe. (C) Difference images [raw MR image (i), and thresholded image (ii)] of a non-ALS mouse administered the anti-DMPO probe (non-ALS-D). (D) Histogram of MRI signal intensity (SI) differences in ALS mice initially administered DMPO and then the anti-DMPO probe (ALS-D), ALS mice administered saline and the anti-DMPO probe (ALS-C) (DMPO control), and non-Tg mice administered DMPO and the anti-DMPO probe (non-ALS-D) (disease control). Data is represented as mean ± S.D.. There was a significant increase in the MR image signal intensity difference for ALS mice administered both DMPO and the anti-DMPO probe compared to the ALS mice administered saline (no DMPO) and the anti-DMPO probe ($p<0.01$) or wild-type controls administered DMPO and the anti-DMPO probe ($p<0.05$). (E) Estimated anti-DMPO probe concentrations (M) calculated from T_1 values in lumbar regions of mouse spinal cords in ALS (ALS mice initially administered DMPO followed by the anti-DMPO probe, ALS-D; and ALS mice initially administered saline instead of DMPO followed by the anti-DMPO probe, ALS-C) and non-Tg

controls (non-ALS mice initially administered DMPO followed by the anti-DMPO probe, non-ALS-D). There was a significant increase in the anti-DMPO probe concentration (M) for ALS mice administered both DMPO and the anti-DMPO probe compared to the ALS mice administered saline (no DMPO) and the anti-DMPO probe ($p<0.0001$) or wild-type controls administered DMPO and the anti-DMPO probe ($p<0.0001$). n=5 for all groups.

Figure 4: *Ex vivo* detection of the anti-DMPO probe in the spinal cords of ALS Tg mice. Fluorescence image of streptavidin-Cy3 (red) which binds to the biotin moiety of the anti-DMPO probe in non-ALS mice (A) and ALS mice (B). (A) non-ALS mouse (- ALS) administered DMPO and subsequently given the anti-DMPO probe. (B) ALS mouse (+ ALS) administered DMPO and subsequently given the anti-DMPO probe. Note that anti-DMPO probe levels are elevated in ALS mouse (compared to wild-type or non-ALS mouse). (C) Fluorescence images of the anti-DMPO probe (red) and the endothelial marker, CD31 (green). Outlined areas in (i) are enlarged in (ii). Note that there is no co-localization of the anti-DMPO probe with endothelial cells. (D) Fluorescence images of the anti-DMPO probe (red) and the neuronal marker, NrCAM (green). Outlined areas in (i) are enlarged in (ii). Note co-localization (yellow) of the anti-DMPO probe with some neuronal cells. For images in (C) and (D) magnification bars for 50 μm (i) and 10 μm (ii) are shown.

Figure 5: *Ex vivo* detection of DMPO nitrone adducts in the spinal cords of ALS Tg mice. Immunohistochemistry (IHC) images of DMPO adducts from excised tissues of animals administered DMPO (no anti-DMPO probe) in non-ALS (- ALS) mouse (Ci,ii) and ALS (+ ALS) mouse (Di,ii). In both of these mice no anti-DMPO probe was administered. Enlarged images shown in (ii) are taken from regions outlined in corresponding (i) images. Note elevated DMPO adducts in ALS mouse (compared to non-ALS mouse). DAPI (blue) stains cell nuclei.

Figure 6: MRI detection of inflammation in lumbar regions of ALS mice. (A) Representative T_2-weighted MR image of a non-Tg control mouse (120 days of age). (B) Representative diffusion-weighted (DW) image of a control mouse. (C) Representative T_2-weighted MR image of an ALS mouse (120 days of age). (D) Representative DW image of an ALS mouse. Note increased signal intensities (oval regions) in lumbar region of ALS mouse with T_2-weighted MR and DW images. Anatomical assignments are: (1) spinal cord, (2) heart, (3) liver, (4) stomach, and (5) intestines. (E) Apparent diffusion coefficients (ADC x 10^{-4} mm^2/s) measured from the lumbar regions of control mice (120 days of age) and ALS mice at 85, 105 and 120 days of age (mean $\pm$ S.D.). There was a significant increase in ADC in ALS mice at 120 days of age compared to controls, as well as a signicant increase for ALS mice at 120 days compared to 85 days of disease progression. n=5 for all groups.

Research Highlights

- *In vivo*, non-invasive detection of free radical-related processes
- Combination of immuno-spin trapping and molecular magnetic resonance imaging
- Application in transgenic mouse model for amyotrophic lateral sclerosis (ALS)
- In vivo detection of free radical adducts in lumbar region of spinal cord
- Validation of trapped radical adducts with *ex vivo* fluorescence microscopic imaging

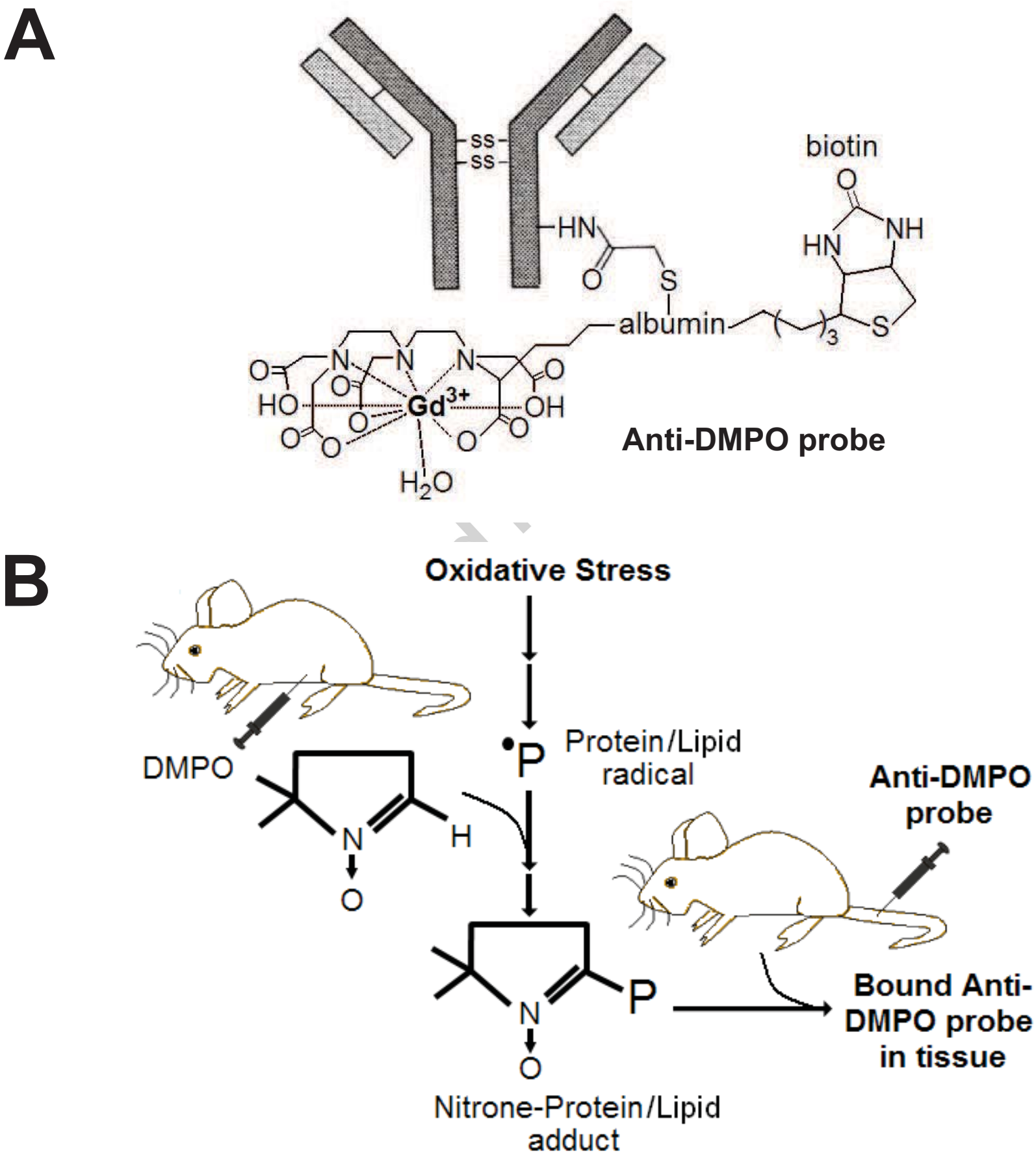

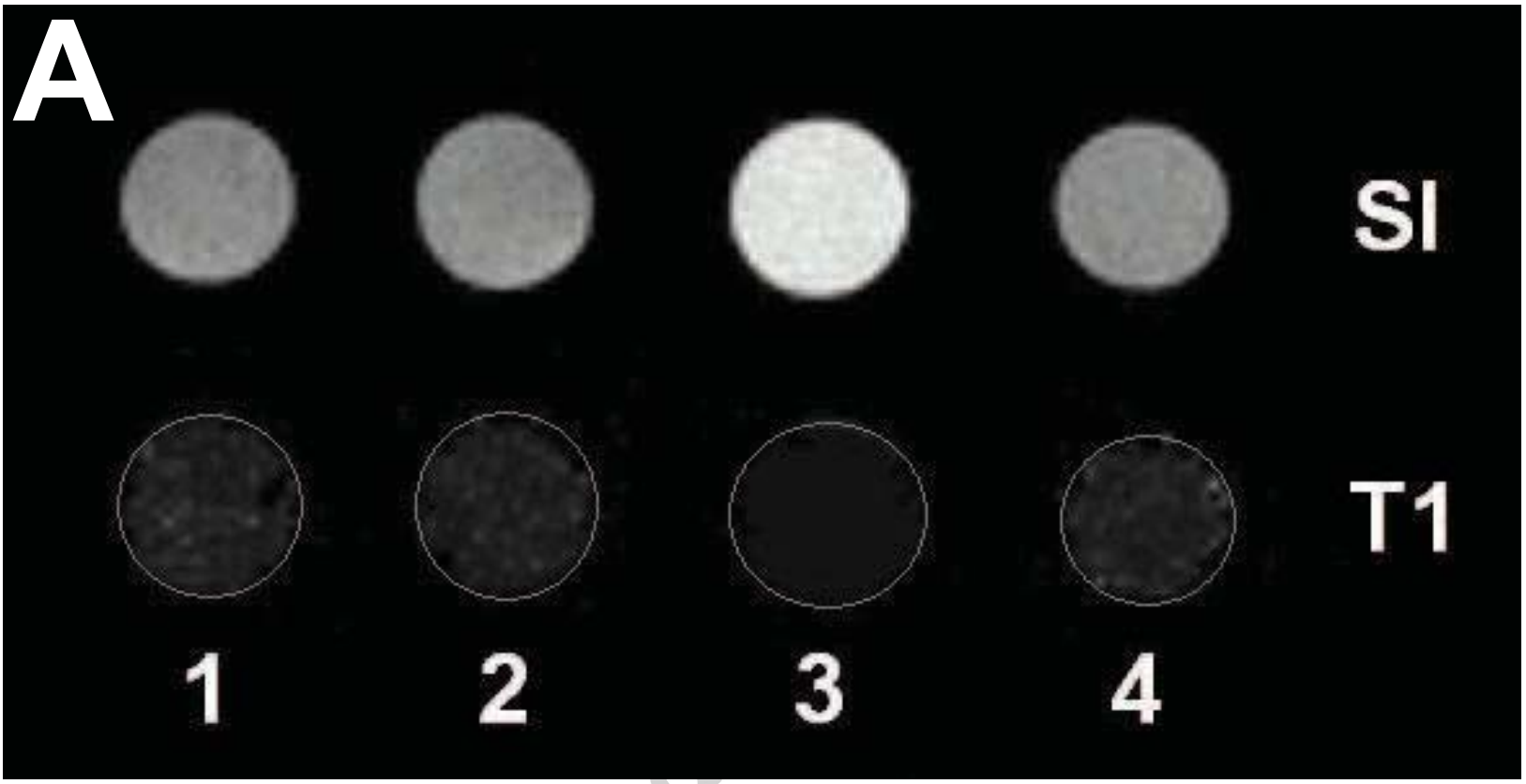

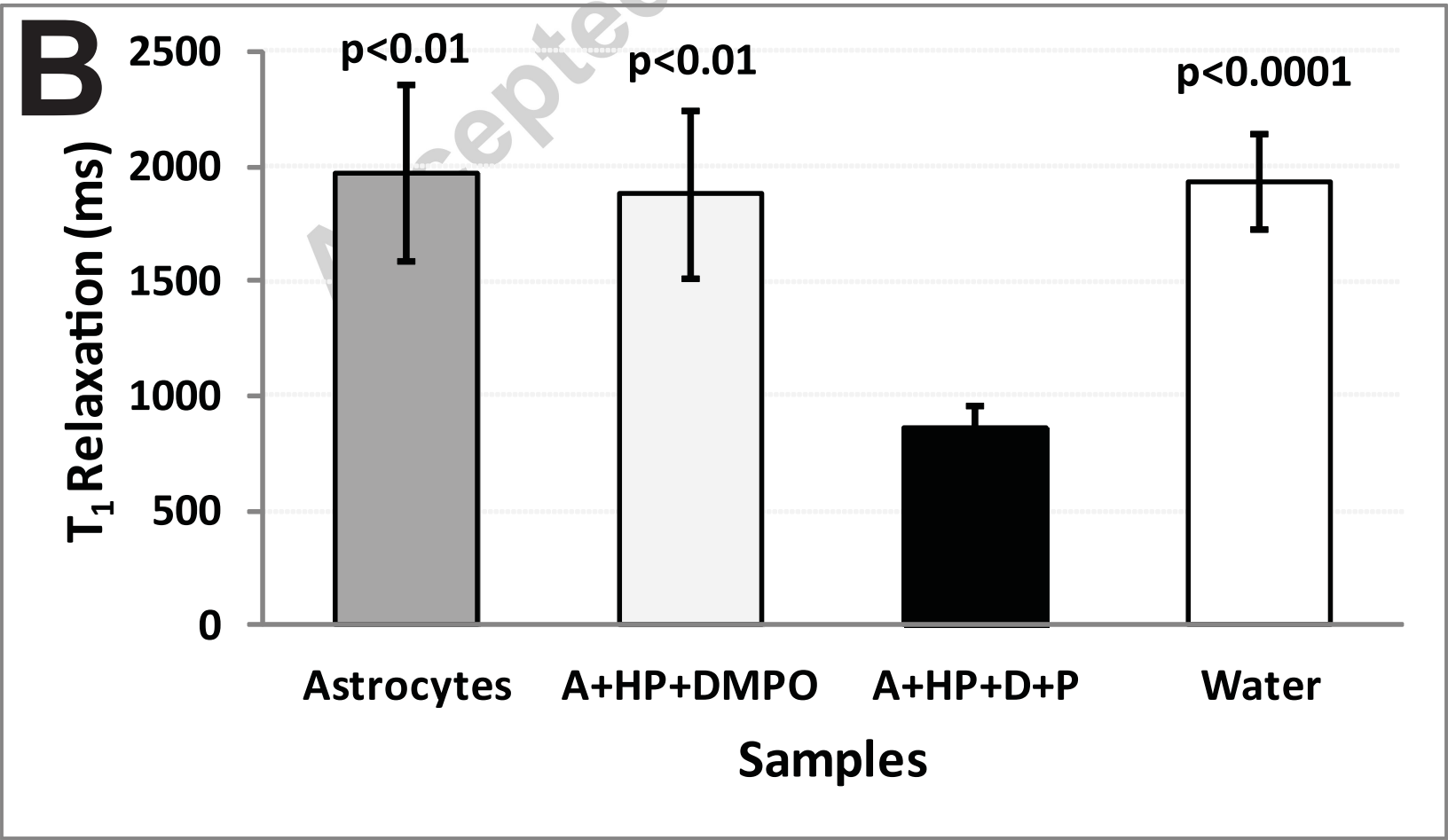

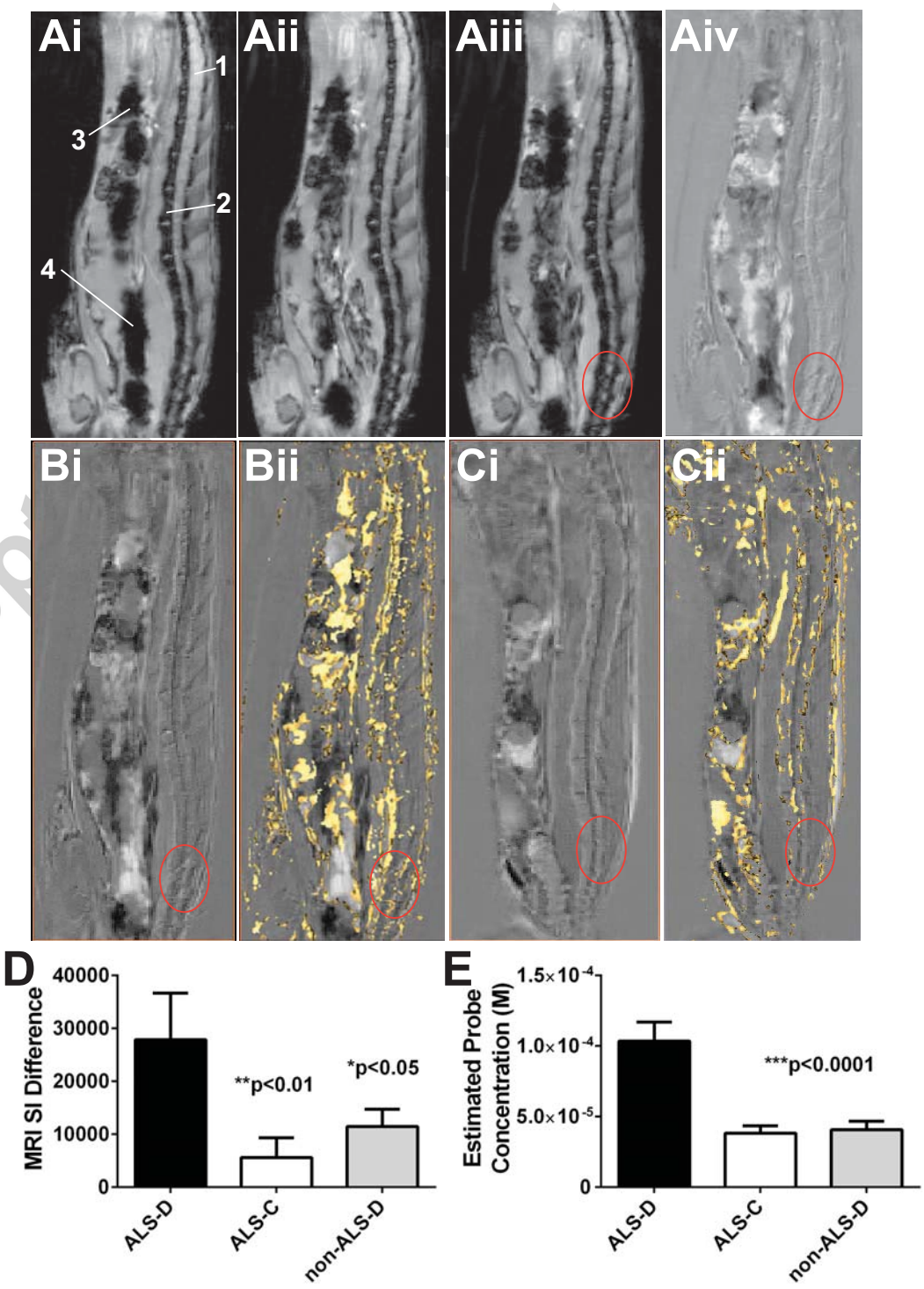

Figure(s)
Click here to download high resolution image